

₁ Study of neutrino-nucleus interaction at around 1 GeV using
₂ hollow cuboid lattice neutrino detectors, WAGASCI, muon
₃ range detectors and magnetized spectrometer, Baby MIND,
₄ at J-PARC neutrino monitor hall

₅ A. Bonnemaison, R. Cornat, L. Domine, O. Drapier, O. Ferreira, F. Gastaldi,
₆ M. Gonin, J. Imber, M. Licciardi, F. Magniette, T. Mueller, L. Vignoli, and O. Volcy

₇ *Ecole Polytechnique, IN2P3-CNRS, Laboratoire Leprince-Ringuet, Palaiseau,*
₈ *France*

₉ S. Cao and T. Kobayashi

₁₀ *High Energy Accelerator Research Organization (KEK), Tsukuba, Ibaraki, Japan*

₁₁ M. Khabibullin, A. Khotjantsev, A. Kostin, Y. Kudenko, A. Mefodiev, O. Mineev,
₁₂ S. Suvorov, and N. Yershov

₁₃ *Institute for Nuclear Research of the Russian Academy of Sciences, Moscow, Russia*

₁₄ B. Quilain

₁₅ *Kavli Institute for the Physics and Mathematics of the Universe (WPI), The*
₁₆ *University of Tokyo Institutes for Advanced Study, University of Tokyo, Kashiwa,*
₁₇ *Chiba, Japan*

₁₈ T. Hayashino, A. Hiramoto, A.K. Ichikawa, K. Nakamura, T. Nakaya, K Yasutome,
₁₉ and K. Yoshida

₂₀ *Kyoto University, Department of Physics, Kyoto, Japan*

₂₁ Y. Azuma, J. Harada, T. Inoue, K. Kin, N. Kukita, S. Tanaka, Y. Seiya,
₂₂ K. Wakamatsu, and K. Yamamoto

₂₃ *Osaka City University, Department of Physics, Osaka, Japan*

24 A. Blondel, F. Cadoux, Y. Favere, E. Noah, L. Nicola, and S. Parsa

25 *University of Geneva, Section de Physique, DPNC, Geneva, Switzerland*

26 N. Chikuma, F. Hosomi, T. Koga, R. Tamura, and M. Yokoyama

27 *University of Tokyo, Department of Physics, Tokyo, Japan*

28 Y. Hayato

29 *University of Tokyo, Institute for Cosmic Ray Research, Kamioka Observatory,*
30 *Kamioka, Japan*

31 Y. Asada, K. Matsushita, A. Minamino, K. Okamoto, and D. Yamaguchi

32 *Yokohama National University, Faculty of Engineering, Yokohama, Japan*

33 December 14, 2017

34 **Contents**

35	1	Introduction	3
36	2	Experimental Setup	4
37	2.1	Wagasci modules	5
38	2.1.1	Detector	5
39	2.1.2	Electronics	8
40	2.1.3	Water system	9
41	2.2	INGRID Proton module	10
42	2.3	Baby MIND	11
43	2.3.1	Magnet modules	11
44	2.3.2	Scintillator modules	13
45	2.3.3	Electronics	14
46	2.3.4	Pefromance check	15
47	2.4	Side muon range detector	15

48	3 Physics goals	18
49	3.1 Expected number of events	19
50	3.2 Pseudo-monochromatic beam by using different off-axis fluxes	19
51	3.3 Subjects Wagasci can contribute	20
52	4 Status of J-PARC T59 experiment	22
53	5 MC studies	26
54	5.1 Simulation setup	26
55	5.2 Event selection	27
56	6 Standalone WAGASCI-module performances	28
57	6.1 Reconstruction algorithm	30
58	6.1.1 Description	30
59	6.1.2 Performances	32
60	6.2 Background subtraction: the water-out module	36
61	7 Schedule	39
62	8 Requests	39
63	8.1 Neutrino beam	39
64	8.2 Equipment request including power line	39

65 **1 Introduction**

66 The understanding of neutrino-nucleus interactions in the 1 GeV energy region is critical
 67 for the success of accelerator-based neutrino oscillation experiments such as the T2K exper-
 68 iment. Complicated multi-body effects of nuclei render this understanding difficult. The
 69 T2K near detectors have been measuring these and significant progress has been achieved.
 70 However, the understanding is still limited. One of the big factors preventing from full
 71 understanding is the non-monochromatic neutrino beam spectrum. Measurements with
 72 different but some overlapping beam spectra would greatly benefit to resolve the contribu-
 73 tion from different neutrino energies. We, the WAGASCI collaboration, proposes to study
 74 the neutrino-nucleus interaction at the B2 floor of the neutrino monitor building, where
 75 different neutrino spectra can be obtained due to the different off-axis position. Our exper-
 76 imental setup contains hollow cuboid lattice plastic-scintillator detectors filled with water
 77 as the neutrino interaction target (WAGASCI modules), two side- and one downstream-
 78 muon range detectors(MRD's). The hollow cuboid lattice and side-MRD's allows a mea-
 79 surement of wider-angle scattering than the T2K off-axis near detector (ND280). High
 80 water to scintillator material ratio enables the measurement of the neutrino interaction on

81 water, which is highly desired for the T2K experiment because it's far detector, Super-
82 Kamiokande, is composed of water. The MRD's consist of plastic scintillators and iron
83 plates. The downstream-MRD, so called the Baby MIND detector, also works as a magnet
84 and provides the charge identification capability as well as magnetic momentum measure-
85 ment for high energy muons. The charge identification is essentially important to select
86 antineutrino events in the antineutrino beam because contamination of the neutrino events
87 is as high as 30%. Most of the detectors has been already constructed. The WAGASCI
88 modules have been commissioned as the J-PARC T59 experiment and the Baby MIND
89 detector was commissioned at the CERN neutrino platform. Therefore, the collaboration
90 will be ready to proceed to the physics data taking for the T2K beam time in January 2019.
91 We will provide the cross sections of the charged current neutrino and antineutrino inter-
92 actions on water with slightly higher neutrino energy than T2K ND280 with wide angler
93 acceptance. When combined with ND280 measurements, our measurement would greatly
94 improve the understanding of the neutrino interaction at around 1 GeV and contribute to
95 reduce one of the most significant uncertainty of the T2K experiment.

96 **2 Experimental Setup**

97 Figure 1 and 2 show a schematic view and a CAD drawing of the entire set of detectors.
98 Central neutrino target detectors consist of two WAGASCI modules and T2K INGRID
99 proton module. Inside the WAGASCI module, plastic scintillator bars are aligned as a
100 hollow cuboid lattice and spaces in the lattice are filled with water for a water-in WAGASCI
101 module. T2K INGRID proton module is a full active neutrino target detector which is
102 composed only with scintillator bars in its tracking region. The central detectors are
103 surrounded by two side- and one downstream- muon range detectors(MRD's) The MRD's
104 are used to select muon tracks from the charged-current (CC) interactions and to reject
105 short tracks caused by neutral particles that originate mainly from neutrino interactions in
106 material surrounding the central detector, like the walls of the detector hall, neutrons and
107 gammas, or neutral-current (NC) interactions. The muon momentum can be reconstructed
108 from its range inside the detector. The MRD's consist of plastic scintillators and iron
109 plates. In addition, each of the iron plates of the downstream-MRD, so called the Baby
110 MIND detector, is wound by a coil and can be magnetized. It provide the charge selection
111 capability.

112 For all detectors, scintillation light in the scintillator bar is collected and transported
113 to a photodetector with a wavelength shifting fiber (WLS fiber). The light is read out by
114 a photodetector, Multi-Pixel Photon Counter (MPPC), attached to one end of the WLS
115 fiber. The signal from the MPPC is read out by the dedicated electronics developed for the
116 test experiment to enable bunch separation in the beam spill. The readout electronics is
117 triggered using the beam-timing signal from MR to synchronize to the beam. The beam-
118 timing signal is branched from those for T2K, and will not cause any effect on the T2K

119 data taking.

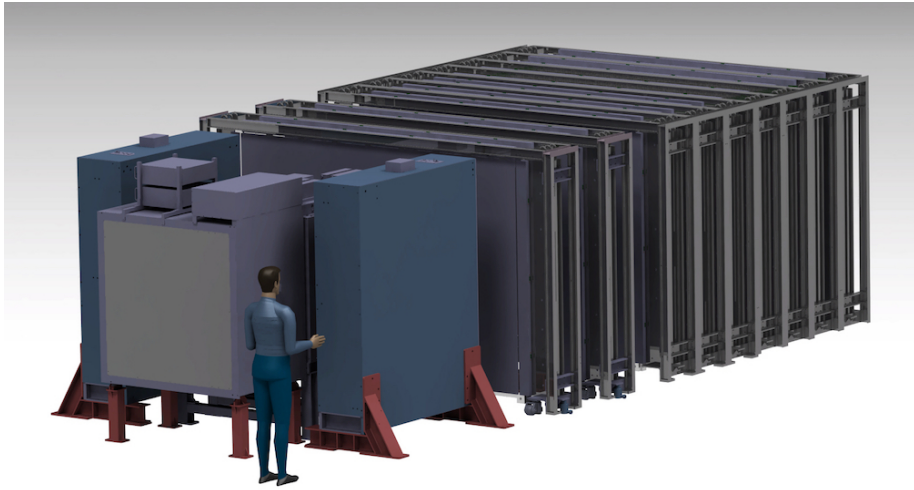


Figure 1: Schematic view of entire sets of detectors.

120 T2K adopted the off-axis beam method, in which the neutrino beam is intentionally
121 directed 2.5 degrees away from SK producing a narrow band ν_μ beam. The off-axis near
122 detector, ND280, is installed towards the SK direction in the B1 floor of the near detector
123 hall of the J-PARC neutrino beam-line. We propose to install our detector in the B2
124 floor of the near detector hall, where the off-axis angle is similar but slightly different: 1.5
125 degree. The candidate detector position in the B2 floor is shown in Figure 3. The expected
126 neutrino energy spectrum at the candidate position is shown in Figure 4.

127 **2.1 WAGASCI modules**

128 **2.1.1 Detector**

129 The WAGASCI modules are mainly composed of 1280 plastic scintillator bars and a sur-
130 rounding stainless steel tank as shown in Figure 5. The total number of channels in one
131 WAGASCI module is 1280. The stainless steel tank is constructed by welding stainless
132 steel plates, is sized as $46 \times 125 \times 125 \text{ cm}^3$, and weighs 0.5 ton.

133 One WAGASCI module consists of 16 scintillator tracking planes, where each plane
134 is an array of 80 scintillator bars fixed with ABS frames. The 40 bars, called parallel
135 scintillators, are placed perpendicularly to the beam, and the other 40 bars, called lattice
136 scintillators, are placed in parallel to the beam with hollow cuboid lattice in the tracking
137 plane as shown in Figure 5. Thanks to the hollow cuboid lattice of the scintillator bars,
138 the WAGASCI module has 4π angular acceptance for charged particles.

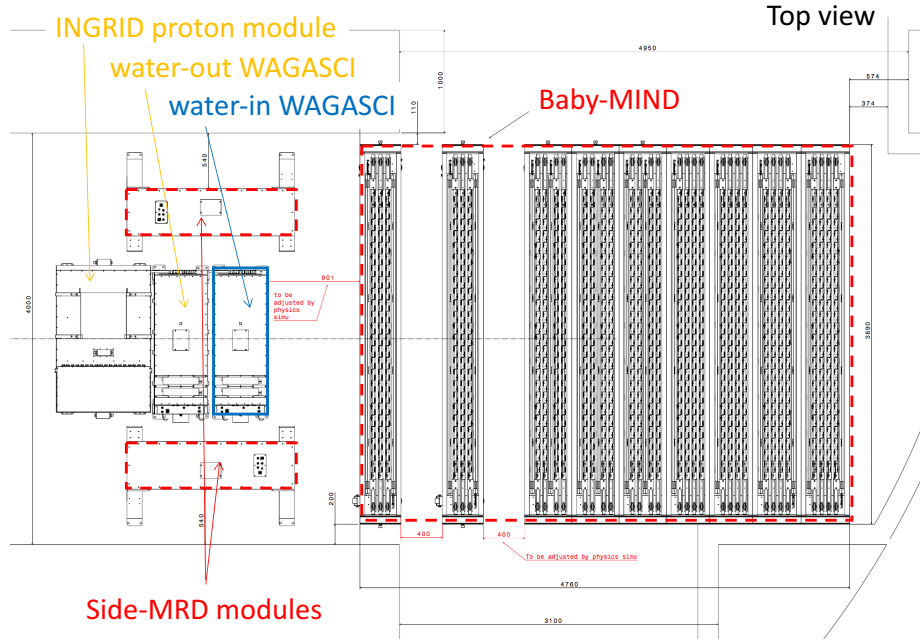


Figure 2: Top view of entire sets of detectors.

139 Thin plastic scintillator bars produced at Fermilab by extrusion method, mainly consists
 140 of polystyrene and are surrounded by thin reflector including TiO_2 (3 mm in thickness)
 141 are used for the WAGASCI modules to reduce the mass ratio of scintillator bars to water,
 142 because neutrino interactions in the scintillator bars are a background for the cross section
 143 measurements on H_2O . Each scintillator bar is sized as $1020 \times 25 \times 3 \text{ mm}^3$ including the
 144 reflector part, and half of all the scintillator bars have 5-cm-interval slits to form the
 145 hollow cuboid lattice (Figure 6).

146 We will have two types of the WAGASCI modules, a water-in module and a water-out
 147 module. The water-in WAGASCI module has water in spaces of the hollow cuboid lattice.
 148 The total water mass serving as neutrino targets in the fiducial volume of the module is
 149 188 kg, and the mass ratio of scintillator bars to water is 80 %. The water-out WAGASCI
 150 module doesn't have water inside the detector. The total CH mass serving as neutrino
 151 target in the fiducial volume of the module is 47 kg, and the mass fraction of scintillator
 152 bars is 100 %.

153 Scintillation light is collected by wave length shifting fibers, Y-11 (non-S type with a
 154 diameter of 1.0 mm produced by Kuraray. A fiber is glued by optical cement in a groove
 155 on surface of a scintillator bar. 32 fibers are gathered together by a fiber bundle at edge
 156 of the module, and lead scintillation light to a 32-channel arrayed MPPC. Since crosstalk

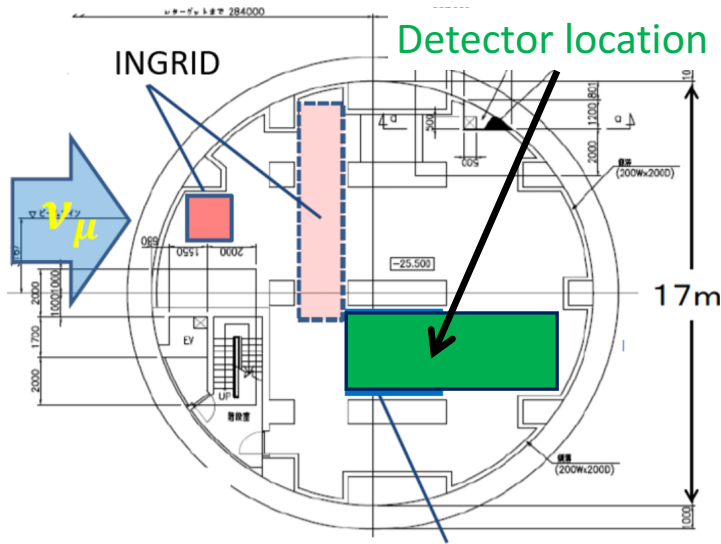


Figure 3: Candidate detector position in the B2 floor of the near detector hall.

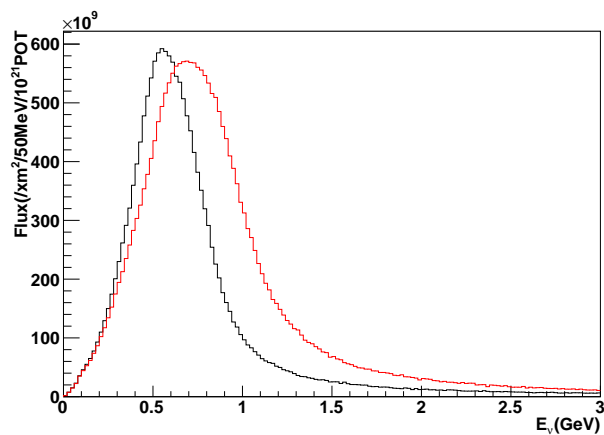


Figure 4: Neutrino energy spectrum at the candidate detector position (red, off-axis 1.5 degree). The spectrum at the ND280 site (black, off-axis 2.5 degree) is also shown.

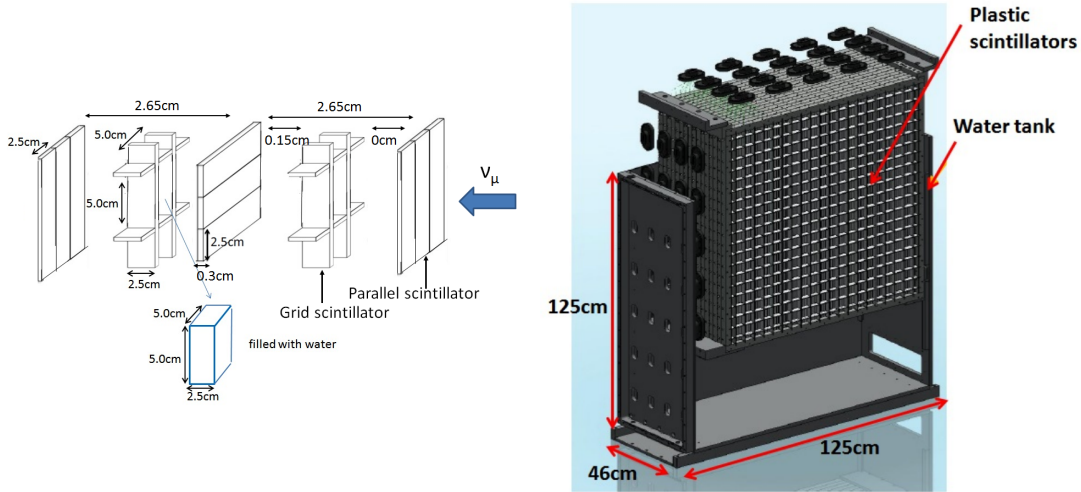


Figure 5: Schematic views of hollow cuboid lattice of plastic scintillator bars (left) and WAGASCI module (right).

of light yield due to reflection on the inner surface of each cell has been observed, all the scintillator bars are painted black by aqueous color spray. It is confirmed by measurements with cosmic rays that black painting on the surface of the scintillator bars suppresses this crosstalk so that no significant crosstalk effect is observed within uncertainty.

32-channel arrayed MPPCs, as shown in the Figure 7, are used for the modules. The surface of the fiber bundle is polished and directly attached onto the 32-channel arrayed MPPCs. The positions of 32 fibers on the bundle are aligned to fit the channels of MPPCs. The MPPC is a product of Hamamatsu Photonics, S13660(ES1), with suppressed noise rate of ~ 6 kHz per channel at 0.5 p.e. threshold. For each MPPC channel, 716 pixels of APD are aligned in a shape of circle.

2.1.2 Electronics

As front-end electronics of this detector, a Silicon PM Integrated Read-Out Chip (SPIROC) [12] is adopted. SPIROC is a 36-channel auto-triggered front-end ASIC, and is produced by OMEGA/ IN2P3. It not only contains an analog signal processing part such as amplification and shaping of the waveform, but contains a digital signal processing parts such as auto-trigger and timing measurement. Charge of MPPC signal is sampled by track-and-hold circuit. A Front-end electronics board, Active Sensor Unit (ASU), has been developed with the SPIROC2D chip, which is the latest version of SPIROC. Each readout board is designed to control a 32-channel arrayed MPPC, and 40 of the ASU boards are aligned on the module surface. The data acquisition system used for this detector, including back-end

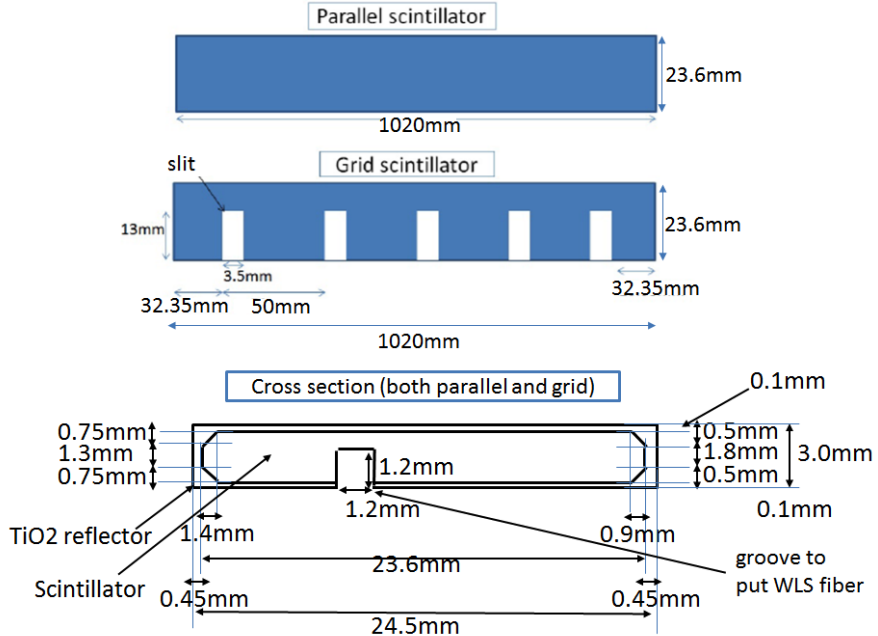


Figure 6: Geometry of scintillators used for WAGASCI modules.

boards, has been developed for prototypes of ultra-granular calorimeters for the International Linear Collider (ILC) [5], and independent of the T2K DAQ system. To synchronize the DAQ system to J- PARC neutrino beam, pre-beam trigger and beam trigger are sent to the clock control card. The beam trigger signals are converted from optical signals to NIM signals at NIM module on the B2 floor. In addition, the information of spill number are delivered with 16-bit ECL level signals, and converted to an Ethernet frame by an FPGA evaluation board to be directly sent to the DAQ PC. The electronics readout scheme is shown in Figure 8.

2.1.3 Water system

Pure water is filled to the water tank of the water-in WAGASCI module as follows. First, the water storage tank located at the B2 floor of the NM pit is filled with water delivered from a water tap on the ground level through a long hose. Second, the water is pumped to the other water storage tank though a water filler to produce pure water. Third, a compound preservative called Germall plus, which is the same preservative used in one of the sub-detectors of T2K ND280, FGD2, is put into the water to keep water from being bad. Then, the water is poured to the water-in WAGASCI module, and it is kept in the module during the neutrino beam operation and not to be circulated.

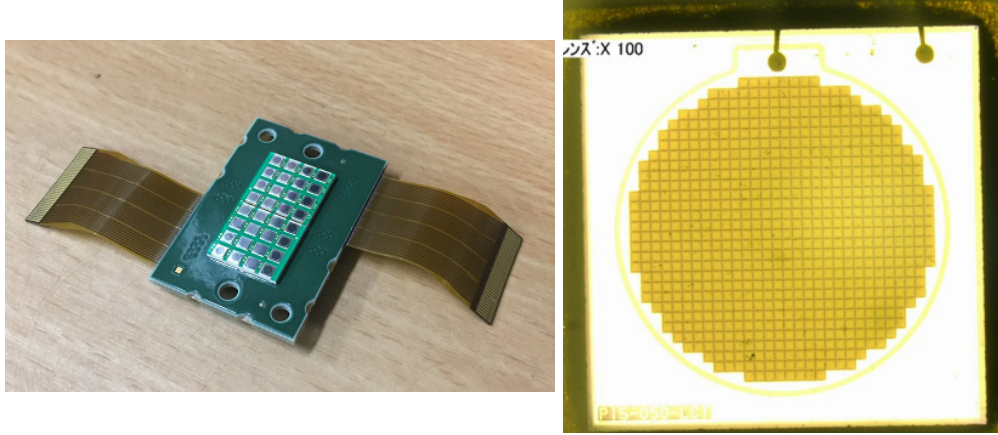


Figure 7: 32-channel arrayed MPPC (left) and an enlarged view of one MPPC channel (right).

2.2 INGRID Proton module

INGRID Proton module is a neutrino detectors of the T2K experiment. It is a fully-active tracking detector which consists of only scintillator strips. The purpose of this Proton Module is to separate the neutrino interaction types by detecting the protons and pions together with the muons from the neutrino interactions, and to measure the neutrino cross section for each interaction type. It consists of 36 tracking planes surrounded by veto planes (Figure 9), where each tracking plane is an array of two types of scintillator strips. The 16 strips in the inner region have dimensions of $2.5\text{cm} \times 1.3\text{cm} \times 120\text{cm}$, while the 16 strips in the outer region have dimensions of $5\text{cm} \times 1\text{cm} \times 120\text{cm}$, making a plane of $120 \times 120\text{cm}^2$ in the horizontal and vertical directions. The former is the scintillator produced for the K2K SciBar detector [3] and the latter was produced for INGRID. The tracking planes are placed perpendicular to the beam axis at 23mm intervals. Since the strips are aligned in one direction, each tracking plane is sensitive to either the horizontal or vertical position of the tracks. The tracking planes are therefore placed alternating in the horizontal and vertical directions so that three-dimensional tracks can be reconstructed. The tracking planes also serve as the neutrino interaction target. As with the WAGASCI modules, scintillation light is read out by a WLS fiber and MPPC.

It was installed at the neutrino beam axis on the SS floor of the T2K near detector hall in 2010, and had been used for neutrino cross section measurements. In August 2017, it was moved to the B2 floor of the T2K near detector hall by J-PARC T59 after getting the approval from T2K to use them. J-PARC T59 is performing a neutrino beam measurement using the detector from October 2017, and the measurement will continue until May 2018 as we will discuss in Sec. 4.

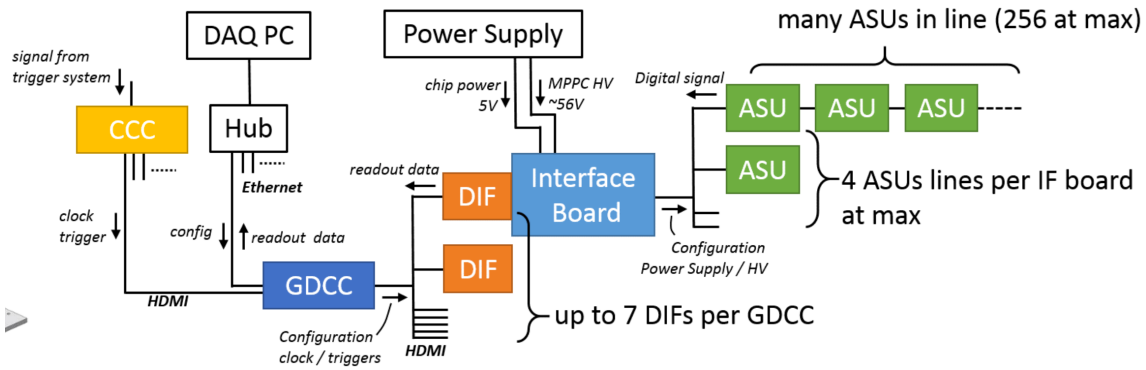


Figure 8: WAGASCI electronics readout scheme.

217 We will operate the INGRID Proton module using the T2K near detector electronics/DAQ system in the same way as J-PARC T59. A proposal to use the module and its
 218 electronics for our project will be submitted to the T2K collaboration.
 219

220 2.3 Baby MIND

221 The Baby MIND is the downstream Muon Range Detector. It also works as a magnet and
 222 provides the charge identification capability as well as magnetic momentum measurement
 223 for high energy muons.

224 The Baby MIND collaboration ¹ submitted a proposal to the SPSC at CERN, SPSC-P-
 225 353. The project was approved by the CERN research board as Neutrino Platform project
 226 NP05 and constructed. The detector consists of 33 magnet modules, each 3500 mm ×
 227 2000 mm × 50 mm (30 mm steel) with a mass of approximately 2 tonnes. Of these magnet
 228 modules, 18 are instrumented with plastic scintillator modules.

229 2.3.1 Magnet modules

230 The Baby MIND is built from sheets of iron interleaved with scintillator detector modules
 231 but unlike traditional layouts for magnetized iron neutrino detectors (e.g. MINOS) which
 232 tend to be monolithic blocks with a unique pitch between consecutive steel segments and
 233 large conductor coils threaded around the whole magnet volume, the Baby MIND iron
 234 segments are all individually magnetized as shown in Figure 10, allowing for far greater
 235 flexibility in the setting of the pitch between segments, and in the allowable geometries
 236 that these detectors can take.

237 The key design outcome is a highly optimized magnetic field map. A double-slit con-
 238 figuration for coil winding was adopted to increase the area over which the magnetic flux

¹Contact person: E. Noah, Spokesperson: A. Blondel, Deputy spokesperson: Y. Kudenko



Figure 9: Schematic view of INGRID Proton module.

lines are homogeneous in B_x across the central tracking region. Simulations show the magnet field map to be very uniform over this central tracking region covering an area of $2800 \times 2000 \text{ mm}^2$, Figure 11. The B_x component dominates in this region, with negligible B_y and B_z . This was confirmed by measuring the field with 9 pick-up coils wound around the first module. Subsequent modules were equipped with one pick-up coil. Test results on the 33 modules show all to achieve the required field of 1.5 T for a current of 140 A, with a total power consumption of 11.5 kW. The polarity of the field map shown in Figure 11 (middle) can be reversed by changing the power configuration.

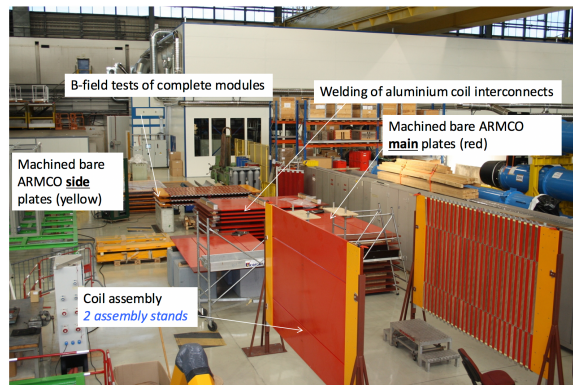


Figure 10: Magnet assembly zone at CERN.

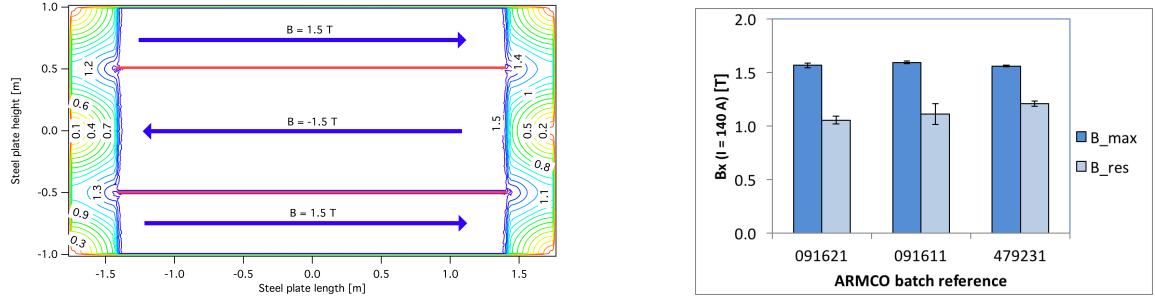


Figure 11: Left) Magnetic field map with a coil along 280 cm of the length of the plate. Right) Measured B field for 33 modules.

246

247 2.3.2 Scintillator modules

248 Each of the 18 scintillator modules is constructed from 2 planes of horizontal counters (95
249 counters in total) and 2 planes of vertical counters (16 counters in total) [2], arranged
250 with an overlap between planes to achieve close to 100% hit efficiency for minimum ionizing
251 muons. The arrangement of planes within a module is vertical-horizontal-horizontal-
252 vertical. This arrangement was the result of an assembly approach whereby each plane
253 was built from 2 half-planes, with each half plane consisting of a horizontal plane and a
254 vertical plane. The scintillator bars are held in place using structural ladders that align
255 and maintain the counters, Figure 12. No glue is used in the process, so counters can be
256 replaced. Aluminum sheets front and back provide light tightness.



Figure 12: Scintillator modules assembly. Left) top of front half-module showing vertical counters, and the spacers-ladders that set the pitch between horizontal counters and hold them in place. Middle) rear half-module showing horizontal counters on their ladders. Right) Assembled rear half-module, the front half-module can be seen in the background.

257 The plastic scintillator counters were made from 220 mm-wide slabs, consisting of
258 extruded polystyrene doped with 1.5% paraterphenyl (PTP) and 0.01% POPOP. They were
259 cut to size then covered with a 30-100 μm thick diffuse reflector resulting from etching of
260 the surface with a chemical agent [9, 10]. The horizontal counter size is $2880 \times 31 \times 7.5 \text{ mm}^3$,

261 with one groove along the length of the bar in which sits a wavelength shifting fiber from
 262 Kuraray. The vertical counter size is $1950 \times 210 \times 7.5$ mm 3 , with one U-shaped groove
 263 along the bar. On each counter, two custom connectors house silicon photomultipliers,
 264 MPPC type S12571-025C from Hamamatsu, either side of the horizontal counter, and
 265 both connectors at the top for the vertical counter. This geometrical configuration for
 266 vertical counters was chosen for ease of connectivity to the electronics, and maintenance
 267 operations.

268 A total of 1744 horizontal counters and 315 vertical counters (including spares) were
 269 produced at the Uniplast company (Vladimir, Russia).

270 2.3.3 Electronics

271 The Baby MIND electronic readout scheme includes several custom-designed boards [11].
 272 The revised version is shown in Figure 13. At the heart of the system is the electronics
 273 Front End Board (FEB), developed by the University of Geneva. The readout system
 274 includes two ancillary boards, the Backplane, and the Master Clock Board (MCB) whose
 275 development has been managed by INRNE (Bulgarian Academy of Sciences) collaborators.

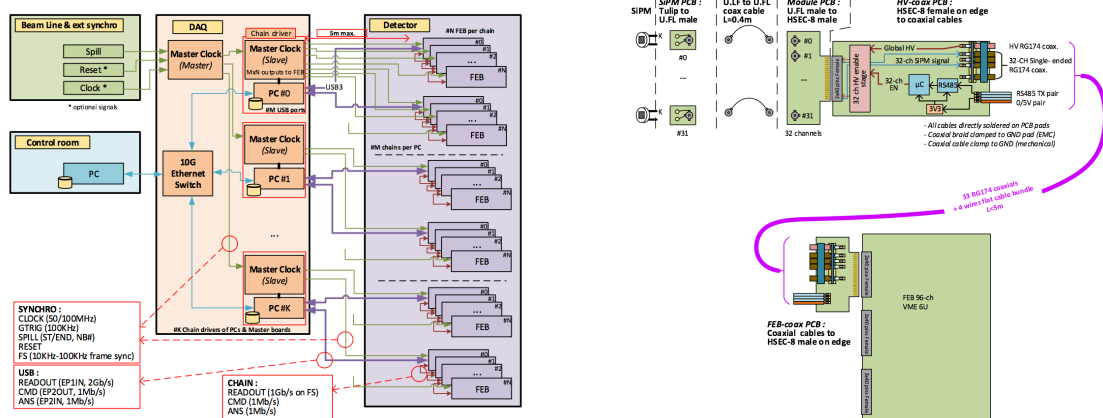


Figure 13: Left) Baby MIND electronics readout scheme. Right) SiPM-to-FEB connectivity.

276 The FEBv2 hosts 3 CITIROC chips that can each read in signals from 32 SiPMs [6].
 277 Each signal input is processed by a high gain, and a separate low gain, signal path. The
 278 outputs from the slow shapers can be sampled using one of two modes: a mode with an
 279 externally applied delay, and a peak detector mode. A faster shaper can be switched to
 280 either HG or LG paths, followed by discriminators with adjustable thresholds providing 32
 281 individual trigger outputs and one OR32 trigger output. An Altera ARIA5 FPGA on the
 282 FEBv2 samples these trigger outputs at 400 MHz, recording rising and falling times for
 283 the individual triggers and assigning time stamps to these. Time-over-threshold from the

284 difference between falling and rising times gives some measure of signal amplitude, used in
285 addition to charge information and useful if there is more than one hit per bar within the
286 deadtime due to the readout of the multiplexed charge output of $\sim 9 \mu\text{s}$. The ARIA5 also
287 manages the digitization of the sampled CITIROC multiplexed HG and LG outputs via a
288 12-bit 8-ch ADC.

289 The internal 400 MHz clock on the FEBv2 can be synchronized to a common 100 MHz
290 clock. The synchronization subsystem combines input signals from the beam line into
291 a digital synchronization signal (SYNC) and produces a common detector clock (CLK)
292 which can eventually be synchronised to an external experiment clock. Both SYNC and
293 CLK signals are distributed to the FEBs. Tests show the FEB-to-FEB CLK(SYNC) delay
294 difference to be 50 ps (70 ps). Signals from the beam line at WAGASCI include two
295 separate timing signals, arriving 100 ms and 30 μs before the neutrino beam at the near
296 detectors. The spill number is available as a 16-bit signal.

297 **2.3.4 Pefromance check**

298 All counters were measured at INR Moscow with a cosmic ray setup using the same type
299 S12571-025C MPPCs and CAEN DT5742 digitizer. The average light yield (sum from both
300 ends) was measured to be 37.5 photo-electrons (p.e.) per minimum ionizing particle (MIP)
301 and 65 p.e./MIP for vertical and horizontal counters, respectively. After shipment to
302 CERN, all counters were tested once more individually with an LED test setup [?]. 0.1% of
303 counters failed the LED tests and were therefore not used during the assembly of modules.
304 The assembly of modules was completed in June 2017, and it was then tested in June and
305 July 2017 at the Proton Synchrotron experimental hall at CERN with a mixed particle
306 beam comprising mostly muons whose momenta could be selected between 0.5 and 5 GeV/c.
307 An event display from the summer 2017 tests is shown in Figure 14.

308 **2.4 Side muon range detector**

309 Two Side-MRD modules for tracking secondary particles from neutrino interactions will be
310 installed in 2018. Each Side-MRD module is composed of 11 steel plates and 10 layers of
311 total 80 scintillator slabs installed in 13 mm gaps between the 30 mm thick plates. Each
312 steel plate size is $30 \times 1610 \times 1800 \text{ mm}^3$. Total module size is $2236 \times 1630 \times 975 \text{ mm}^3$ as
313 shown in Figure 15 (left), weight is ~ 8.5 ton.

314 Scintillator bars were manufactured by Uniplast company in Vladimir, Russia. Polystyrene
315 based scintillators were extruded with thickness of 7 mm, then cut to the size of $7 \times 200 \times$
316 1800 mm^3 . Dopant composition is 1.5% PTP and 0.01% POPOP. Scintillator surface was
317 etched by a chemical agent to form a white diffuse layer with excellent reflective perfor-
318 mance. Ideal contact between the scintillator and the reflector raises the light yield up to
319 50% comparing to an uncovered scintillator. Sine like groove was milled along the scin-
320 tillator to provide uniform light collection over the whole scintillator surface. WLS Y11

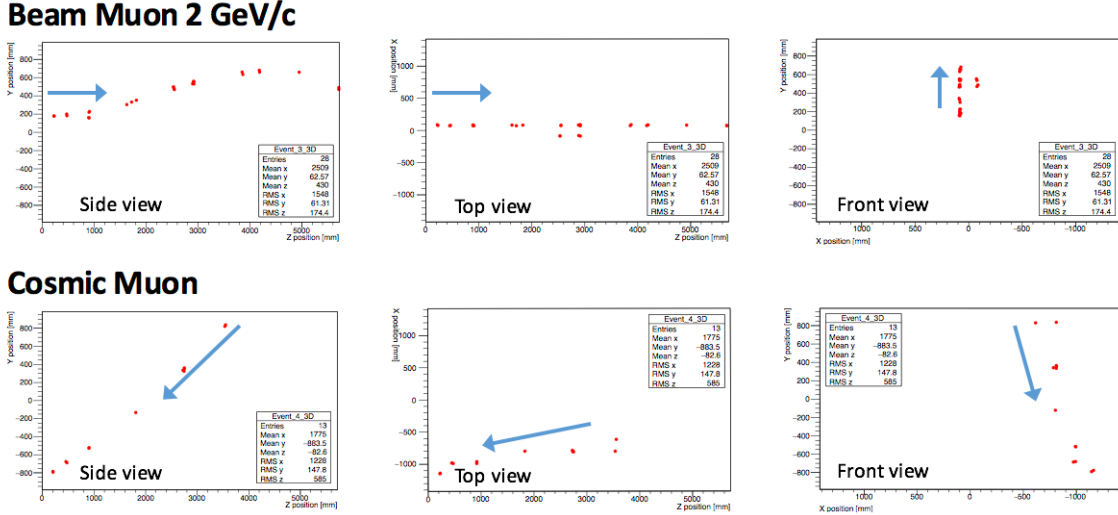


Figure 14: Comparison of a beam muon and cosmic muon in the three different geometrical projections of the detector. The beam impinges on the detector from the left. The arrows indicate the direction of travel of these muons. The direction of the cosmic muon is inferred from timing information.

321 Kuraray fiber of 1 mm diameter is glued with an optical cement EJ-500 in the S-shape
 322 groove as shown in Figure 15(right). Bending radius is fixed to 30 mm that was specified to
 323 be safe for Kuraray S-type fibers. Both ends of the fiber are glued into optical connectors
 324 which mounted within a scintillator body and provide an interface to SiPMs, Hamamatsu
 325 MPPC S13081-050CS(X1).

326 Scintillators for the Side-MRD modules had been assembled at INR in Russia, and
 327 shipped to Japan in July 2017. The light yield for each scintillator was measured with
 328 cosmic rays at INR and at YNU in Japan after delivery. Parameters measured at the
 329 center of the counter were : the light yields LY_1 and LY_2 at both ends, the light yield
 330 asymmetry between the ends calculated as $100\% \times \frac{LY_1 - LY_2}{LY_1 + LY_2}$. After tests at INR we selected
 331 324 counters from measured 332 ones with the mean light yield of 45 p.e./MIP ($LY_1 +$
 332 LY_2) and the asymmetry value less than 10 %. The measurements at YNU yielded the
 333 average total light yield of about 40 p.e./MIP which varies in range from 32 to 50 p.e./MIP
 334 (Figure 16 (left)). Only two counters showed relatively high asymmetry close to 25 % as
 335 shown in Figure 16 (right). Using the results of the quality assurance test we selected 320
 336 scintillator counters for the Side-MRD modules.

337 We also measured the time resolution for a combination of four counters piled each on
 338 another one. The average result for four counters is $\sigma_T = 1.04$ ns. The resolution of com-
 339 bination of 2, 3, 4 counters is measured to be 0.79 ns, 0.66 ns and 0.58 ns, correspondently.

340

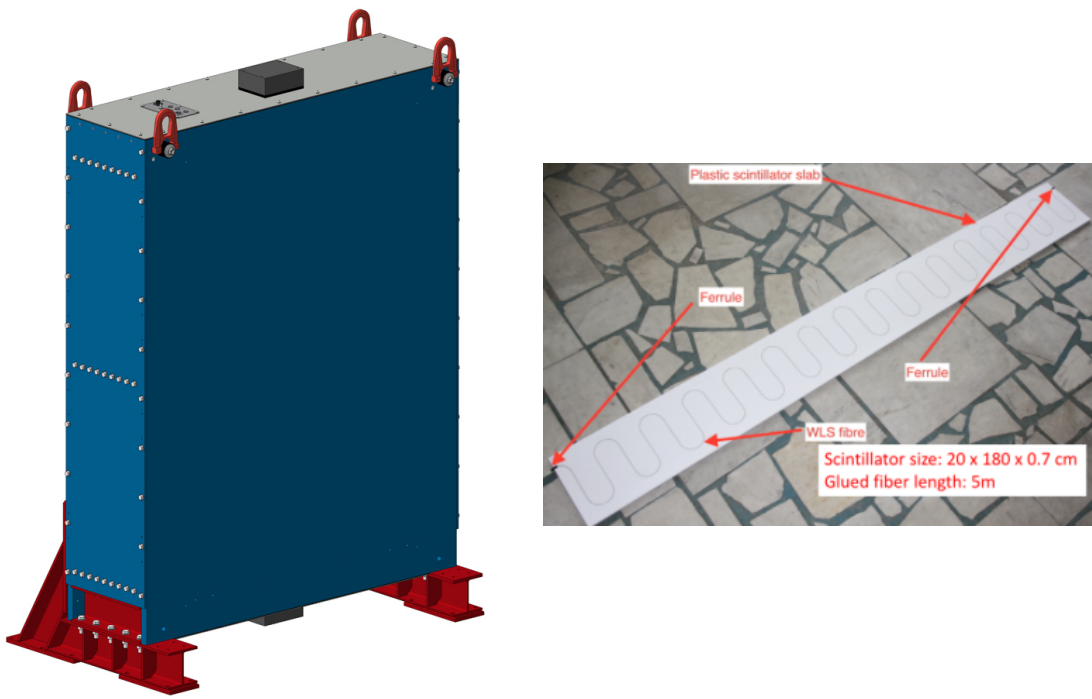


Figure 15: Left :Side-MRD module. Right: Scintillator bar of the Side-MRD modules.

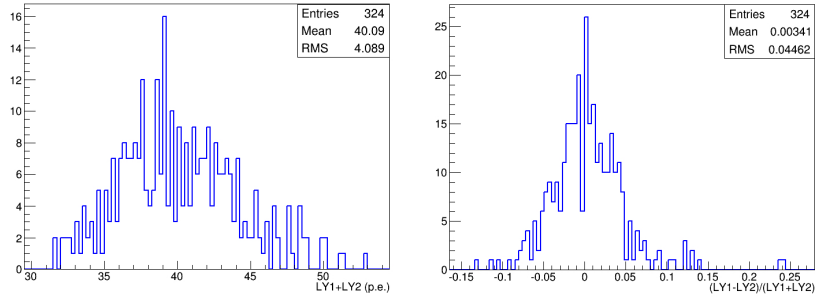


Figure 16: Total light yield distribution (left) and light yield assymetry (right) measured at YNU.

341 Construction of Side-MRD modules will be done from November 2017 at Yokohama
 342 National University, then they will be transported to J-PARC and will be installed at B2
 343 floor of the T2K near detector hall.

344 Same electronics as the WAGASCI modules (see Sec. 2.1.2) are used for the Side-MRD
 345 modules.

346 3 Physics goals

347 We will measure the differential cross section for the charged current interaction on H₂O
 348 and Hydrocarbon(CH)). The water-scintillator mass ratio of the WAGASCI module is as
 349 high as 5:1 and the high purity measurement of the cross section on H₂O is possible. One
 350 experimental option is to remove water from one of the two WAGASCI modules. The
 351 water-out WAGASCI module will allow to measure pure-CH target interactions with very
 352 low momentum-threshold for protons. It will also benefit to subtract the background from
 353 interaction with scintillator in the water target measurement. Another option is to add
 354 the T2K proton module which is fully made of plastic scintillators. It will allow the high
 355 statistics comparison of cross section between H₂O and CH and also comparison with
 356 the ND280 measurement. The actual configuration will be optimized with detailed MC
 357 simulation by 2018 Summer.

358 Our setup allows the measurements of inclusive and also exclusive channels such as 1- μ ,
 359 1- μ 1p, 1- μ 1 $\pi \pm np$ samples, former two of which are mainly caused by the quasi-elastic and
 360 2p2h interaction and the latter is mainly caused by resonant or coherent pion production
 361 and deep elastic scattering. In general, an accelerator produced neutrino beam spectrum
 362 is wide and the energy reconstruction somehow rely on the neutrino interaction model.
 363 Therefore, recent neutrino cross section measurement results including those from T2K
 364 are given as a flux-integrated cross section rather than cross sections as a function of

365 the neutrino energy to avoid the model dependency. We can provide the flux-averaged
366 cross section. In addition, by combining our measurements with those at ND280, model-
367 independent extraction of the cross section for narrow energy region becomes possible.
368 This method was demonstrated in [1] and also proposed by P** (NUPRISM).

369 **3.1 Expected number of events**

370 Expected number of neutrino events after the event selections is evaluated with Monte
371 Carlo simulations as we will discuss in Section 5. In the neutrino-mode, 4.2×10^3 , 1.1×10^3
372 and 3.8×10^3 CC neutrino events are expected in the water-in WAGASCI module, the
373 water-out WAGASCI module and the INGRID proton module after the selections with
374 0.5×10^{21} POT, and its purities are 78.0 %, 97.5 % and $\sim 98\%$. In the antineutrino-mode,
375 1.7×10^3 , 0.4×10^3 and 1.5×10^3 CC antineutrino events are expected in the water-in
376 WAGASCI module, the water-out WAGASCI module and the INGRID proton module
377 after the selections with 0.5×10^{21} POT, and its purities are 59.5 %, 74.4 % and $\sim 74\%$.

378 Statical errors of flux integrated CC-inclusive neutrino cross section measurements on
379 H₂O (full acceptance) and CH targets (forward acceptance) will be 1.5 % and 1.6 % with
380 0.5×10^{21} POT in the neutrino-mode. Statical errors of flux integrated CC-inclusive anti-
381 neutrino cross section measurements on H₂O (full acceptance) and CH targets (forward
382 acceptance) will be 2.4 % and 2.5 % with 0.5×10^{21} POT in the antineutrino-mode.

383 Statical errors of flux integrated H₂O to CH CC-inclusive neutrino cross section ratio
384 measurement will be 3.1 % (full acceptance) and 2.3 % (forward acceptance) with 0.5×10^{21}
385 POT in the neutrino-mode. Statical errors of flux integrated H₂O to CH CC-inclusive
386 antineutrino cross section ratio measurement will be 5 % (full acceptance) and 3.7 %
387 (forward acceptance) with 0.5×10^{21} POT in the antineutrino-mode.

388 **3.2 Pseudo-monochromatic beam by using different off-axis fluxes**

389 The off-axis method gives narrower neutrino spectrum, and the peak energy is lower for
390 larger off-axis angle. There still remains high energy tail mainly due to neutrinos from
391 Kaon decay. The off-axis angle of the WAGASCI location is 1.5 degree and different from
392 the ND280 2.5 degree. Top two plots of Figure 17 show the energy spectra of fluxes and
393 neutrino interaction events at these two different location. The high energy tail of ND280
394 flux can be somehow subtraction by using the WAGASCI measurement. The low energy
395 part of the WAGASCI flux can be also subtracted by using the ND280 measurement.
396 Bottom two plots of Figure 17 demonstrate this method. We can effectively get two fluxes,
397 from 0.2 GeV to 0.9 GeV and 0.6 GeV and 2 GeV and measure flux-integrated cross section
398 for these two fluxes.

399 Statical errors of flux integrated CC-inclusive neutrino cross section measurements
400 on H₂O (forward acceptance) and CH targets (forward acceptance) with the pseudo-
401 monochromatic beam will be 2 % and 1.9 % with 0.5×10^{21} POT in the neutrino-mode.

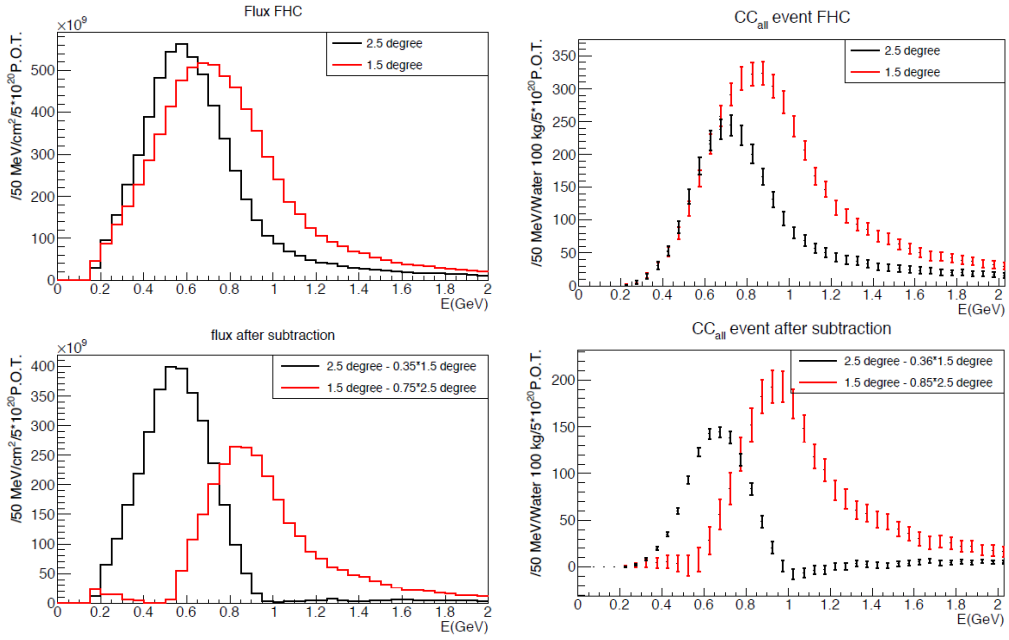


Figure 17: Energy spectra obtained by using different off-axis angle fluxes. Top two plots show the fluxes(left) and spectra of interaction events (right) for ND280 (off-axis 2.5 degree) and WAGASCI (off-axis 1.5 degree). Bottom two plots show the fluxes (left) and spectra of interaction events (right) obtained by subtraction of fluxes at ND280 and WAGASCI. The error bar is for the statistical error and those in the bottom right plot is obtained assuming the statistical error for ND280 measurement is much smaller than that of WAGASCI experiment.

402 Statical errors of flux integrated CC-inclusive antineutrino cross section measurements
 403 on H₂O (forward acceptance) and CH targets (forward acceptance) with the pseudo-
 404 monochromatic beam will be 3 % and 2.8 % with 0.5×10^{21} POT in the neutrino-mode.

405 3.3 Subjects WAGASCI can contribute

406 In T2K experiment, neutrinos interact with bound nucleons in relatively heavy nuclei
 407 (Carbon and Oxygen), so the cross-section is largely affected by nuclear effects. The nuclear
 408 effects are categorized as nucleons' momentum distribution in nucleus, interactions with
 409 correlated pairs of nucleons in nucleus (two particles-two holes, 2p2h), collective nuclear
 410 effects and final state interactions (FSI) of secondary particles in the nuclei after the initial
 411 neutrino interactions.

412 The 2p2h interactions mainly happen through Δ resonance interactions following a

413 pion-less decay and interactions with a correlated nucleon pair. The 2p2h interactions are
 414 observed in electron scattering experiments [7] where the 2p2h events observed in the gap
 415 between Quasi-Elastic region and Pion-production region as shown in Figure 18. Neutrino
 416 experiments also attempt to measure the 2p2h interactions, but separation of the QE peak
 417 and the 2p2h peak is more difficult because transferred momentum (p) and energy (w)
 418 are largely affected by neutrino energies which cannot be determined event-by-event in the
 419 wide energy spectrum of the accelerator neutrino beam. Our model-independent narrow
 420 neutrino spectra extracted from combined analyses of our data and ND280 data are ideal
 421 for searching the 2p2h interaction because clearer separation of the QE peak and the 2p2h
 422 peak is expected. Another way to observe the 2p2h interaction is direct measurement of
 423 proton tracks in CC0 π sample with low detection threshold and full acceptance. Figure 19
 424 shows proton multiplicities after FSI in CCQE events and 2p2h events, and Figure 19 shows
 425 opening angles among two proton tracks in the same samples. The water-out WAGASCI
 426 can provide good sample for the 2p2h interaction search because its low density medium
 427 enables the detection of low momentum protons in addition to the full acceptance.

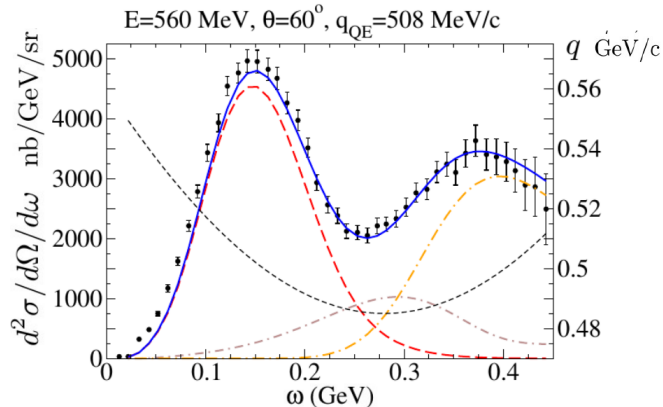


Figure 18: Comparison of inclusive $^{12}\text{C}(\text{e},\text{e}')$ cross sections and predictions of the QE-SuSAv2 model (long-dashed red line), 2p-2h MEC model (dot-dashed brown line) and inelastic-SuSAv2 model (long dot-dashed orange line) (from Ref. [7]). The sum of the three contributions is represented with a solid blue line. The q dependence with ω is also shown (short-dashed black line.)

428 There are various models which describe the collective nuclear effects [8]. The Q^2
 429 dependence of the effects can be tested by measuring angular distribution of muons in
 430 CC1- μ and CC1- $\mu 1p$ events. The uncertainties of the effects in low (high) Q^2 regions can
 431 be constrained by observing the events with a forward-going (high-angle) muon, so it is
 432 essential to measure muon tracks with full acceptance.

433 T2K experiment is starting to use ν_e CC1 π events for its CP violation search to increase

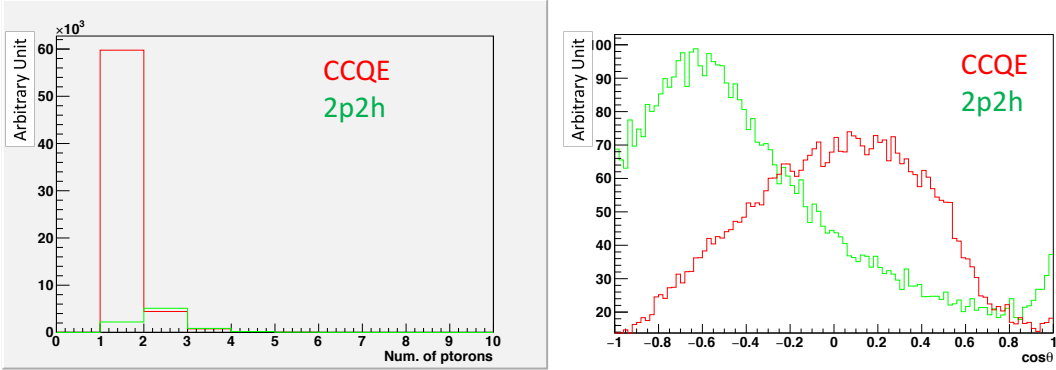


Figure 19: Proton multiplicities (left) and opening angles among two proton tracks (right) after FSI in CCQE events and 2p2h events.

434 the statistics. One of the biggest uncertainty of the CC 1π sample comes from the final
 435 state interactions of pions in the nuclei after the initial neutrino interactions because they
 436 change the multiplicity, charge and kinematics of the pions. The multi-pion production
 437 events can be migrated into the CC 1π sample due to the FSIs, and they become important
 438 backgrounds. We can constrain the uncertainties from the pion FSIs by measuring pion
 439 rescattering in the detector and pion multiplicity in ν_μ CC $n\pi$ sample with low detection
 440 threshold and full acceptance for pion tracks. The water-out WAGASCI can provide good
 441 sample for the pion FSI studies because its low density medium enables the detection of
 442 low momentum pions in addition to the full acceptance.

443 4 Status of J-PARC T59 experiment

444 We had submitted a proposal of a test experiment to J-PARC in April 2014 to test a new
 445 detector with a water target, WAGASCI, at the neutrino monitor hall, and the proposal
 446 was approved as J-PARC T59. The project contains the side and downstream muon range
 447 detectors as well.

448 The first WAGASCI module has been constructed in 2016 and installed at the on-
 449 axis position in front of the T2K INGRID detector for the commissioning and the first
 450 cross section measurement as a part of the T2K experiment. The INGRID electronics
 451 boards are used to read the signal. The light yield measured with muons produced by
 452 the interaction of neutrinos in the hall wall, shown in Figure 20, is sufficiently high to get
 453 good hit efficiency. A track search algorithm based on the cellular automaton has been
 454 developed using the software tools by the T2K INGRID. Examples of observed events are
 455 shown in Figure 21. The tracking efficiency in 2-dimensional projected plane was evaluated

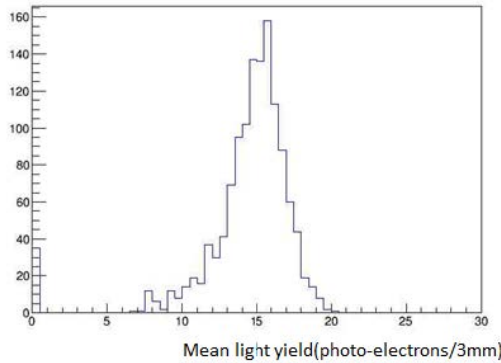


Figure 20: Light yield for muons produced by the interaction of neutrinos in the hall wall. Average light yields for each channel are plotted.

456 by comparing the reconstructed track in the WAGASCI module and the INGRID module
 457 and shown in Figure22. Note that that the tracking efficiency for high angle (> 70 deg)
 458 is not evaluated because of the acceptance of the INGRID module, not because of the
 459 limitation of the WAGASCI module.

460 In 2017 Autumn, the construction of the second WAGASCI module and the dedicated
 461 electronics board were completed. The module and the electronics were install to the B2
 462 floor together with the T2K proton module and the INGRID module as shown in Figure 23.
 463 The proton module is to be used as the entering muon veto and also for the comparison
 464 of interaction between CH and Water. The INGRID module is for the temporary muon
 465 detector with limited acceptance for this period. The detector was commissioned and is
 466 in operation to take data with the antineutrino beam during the T2K beam time from
 467 October.

468 The production of the components of the side muon range detectors has been completed
 469 and now the detectors are being assembled at the Yokohama National University. These
 470 detectors will be installed sometime from January to June, 2018 when T2K is not running.

471 The Baby MIND detector was transported from CERN to Japan in December, 2017.
 472 It will be installed and commissioned in Jan.-Feb. 2018 and T59 will take the neutrino-
 473 induced muon data in April and May.

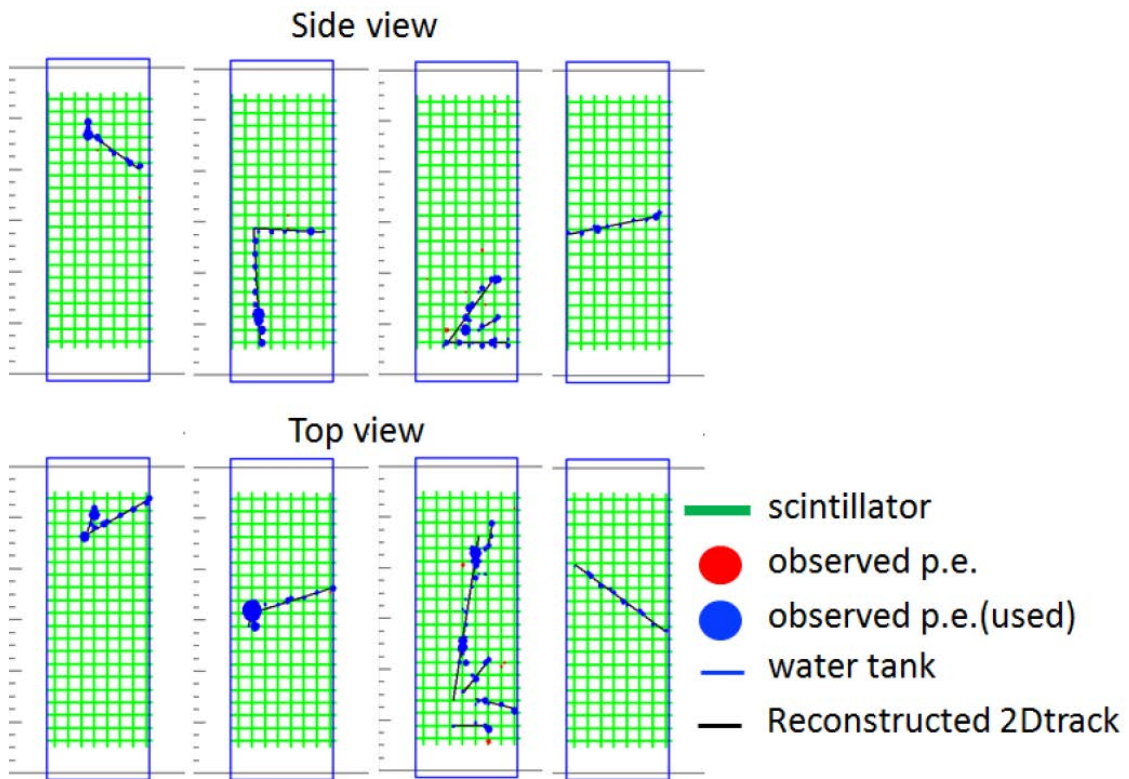


Figure 21: Example event displays of the WAGASCI module at on-axis. The reconstructed tracks are overlaid.

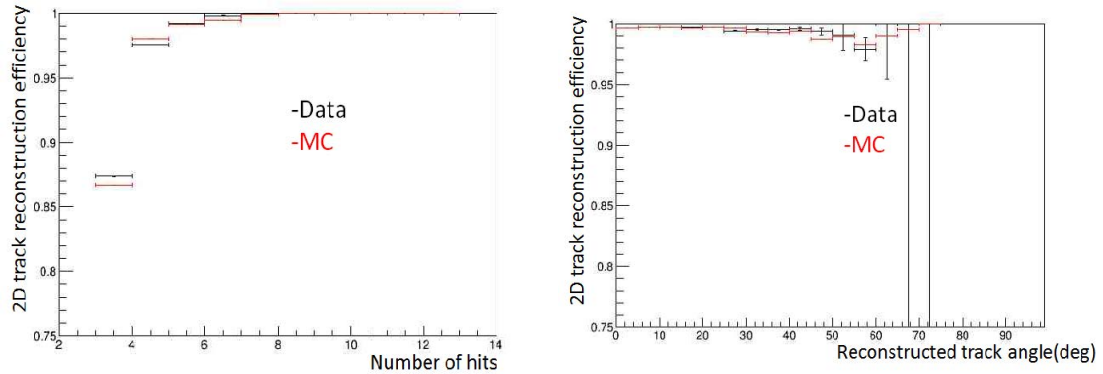


Figure 22: 2D track reconstruction efficiency as a function of number of hits (left) and track angle (right). Here the track angle is the one reconstructed by the INGRID module.

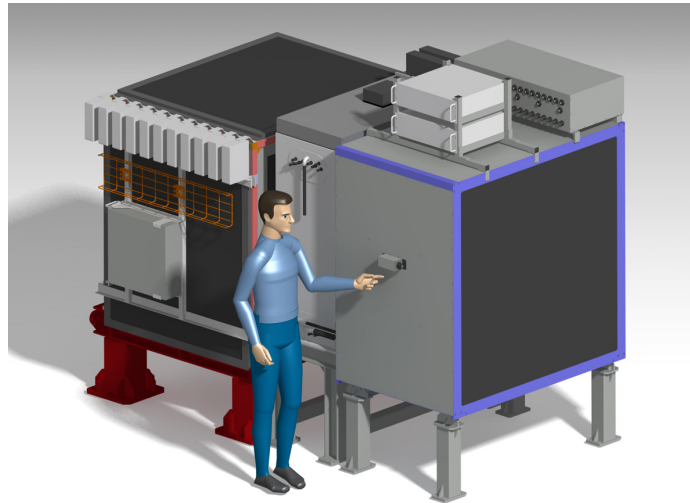


Figure 23: J-PARC T59 detector configuration in October 2017.

474 **5 MC studies**

475 **5.1 Simulation setup**

476 Simulation study was conducted by using the T2K neutrino flux generator, JNUBEAM,
477 neutrino interaction simulator, NEUT, and Geant4 for the detector responses.

478 The detector geometry in the simulation so far is different from the actual setup as
479 shown in Figure 24. The active neutrino target region consists of four WAGASCI modules.
480 The size of the WAGASCI module is same as the actual one: 100 cm × 100 cm in the
481 x and y directions and 50 cm along the beam direction (z-direction). Two Side-MRD
482 modules is installed at both sides of the WAGASCI modules, and each Side-MRD module
483 consists of ten iron plates whose dimension is 3 cm (thickness) × 200 cm (height) × 320 cm
484 (width). The distance between the Side-MRD modules and WAGASCI modules is 80 cm.
485 The downstream-MRD is equivalent to the Baby-MIND, but without the magnetic field.
486 It consists of thirty iron plates whose dimension is 3 cm (thickness) × 200 cm (height)
487 × 400 cm (width). The distance between the downstream-MRD modules and WAGASCI
488 modules is 80 cm. Update of the study with the actual geometry is now underway.

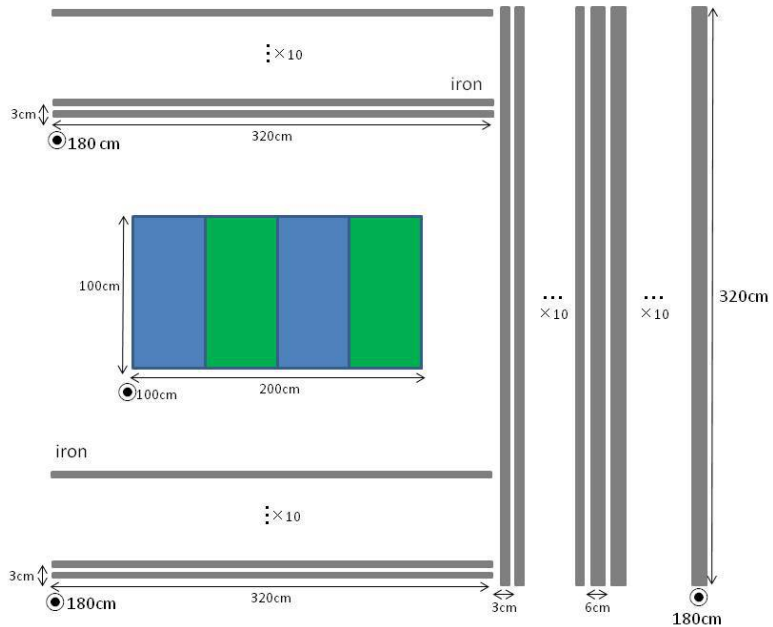


Figure 24: Geometry of the detectors in the Monte Carlo simulation.

489 To simulate the signal, the energy deposit inside the scintillator is converted into the

490 number of photons. The effects of collection and attenuation of the light in the scintillator
491 and the WLS fiber are simulated, and the MPPC response is also taken into account. The
492 light yield is smeared according to statistical fluctuations and electrical noise.

493 **5.2 Event selection**

494 Tracks are reconstructed in two-dimensional planes in each sub-detector. Then, track
495 matching among the sub-detectors and three-dimensional track reconstruction are per-
496 formed. These analysis tools have been developed from the software tools by the T2K
497 INGRID and in mature stage already.

498 The events are selected as follows. The starting point of the track is required to be
499 5 cm away from the edge of the WAGASCI module. This is to remove the background
500 from the outside. The longest track has to penetrate more than one (five) iron plates in
501 Side-MRD modules (Baby-MIND). This cut select a muon track and rejects backgrounds
502 from NC and neutral particles. Then, in order to determine the muon momentum, it is
503 required that the longest track stops in MRDs (Side-MRD modules and Baby-MIND) or
504 penetrate all iron plates.

505 Table 1 shows numbers of the selected events in one water-in WAGASCI module after
506 the event selection. We expect 4,239 (1,666) events from charged-current interaction on
507 water with 5×10^{20} POT in (anti)neutrino-mode with one water-in WAGASCI module.
508 The purity, when interactions on CH is counted as background, is 78% for the neutrino-
509 mode. There is a significant contamination from the wrong-sign (neutrino) interaction for
510 antineutrino-mode, however, we expect that it will be removed with efficiency higher than
90% by Baby MIND.

Table 1: Expected number of the selected neutrino-candidate events in one water-in WA-
GASCI module with 5×10^{20} POT in each of neutrino-mode and antineutrino-mode. Note
that the wrong sign component will be reduced by one order by applying the charge selec-
tion by Baby MIND.

	CC on water	NC on water	Interaction on CH	wrong sign interaction
ν -mode	4239	107	1087	(negligible)
anti- ν -mode	1666	14	560	(561)

511
512 Table 2 and 3 summarize contributions classified by the interaction types and final state
513 topologies for the selected charged current-interaction events, respectively.

514 Figure 25 shows the reconstructed angles of the longest tracks in the selected events in
515 the neutrino-mode and the anti-neutrino mode. Figure ?? shows the iron plane numbers
516 in Side-MRD and Baby-MIND corresponding to the end points of the longest tracks in the
517 selected events in the neutrino-mode and the anti-neutrino mode.

Table 2: Interaction types for the selected charged-current events.

	CCQE	2p2h	CC resonant π	CC-DIS
ν -mode	48.4 %	9.7 %	27.1 %	14.7 %
anti- ν -mode	57.1 %	8.2 %	17.3 %	17.3 %

Table 3: Final state topologies for the selected charged-current events.

	CC0 π	CC1 π	CC2 π	CCn π
ν -mode	67.4 %	20.9 %	3.0 %	8.7 %
anti- ν -mode	79.5 %	16.3 %	1.2 %	3.0 %

518 6 Standalone WAGASCI-module performances

519 In the previous sections, the WAGASCI detector was studied using the Muon Range Detectors. In this section, the standalone abilities of WAGASCI module are presented. Using
520 the WAGASCI configuration presented in Section 5, we have evaluated that only 7% of
521 the muons will be stopped in one of the WAGASCI modules. However, this proportion
522 increases to 53% for pions and 73% for protons produced by neutrino interactions at 1.5°
523 off-axis. Figure 27 shows the momentum distribution of these daughter particles as well as
524 for the sub-sample stopped in one of the WAGASCI modules. Therefore, the study of the
525 standalone abilities of the WAGASCI module in this section are dominantly motivated by:
526

- 527 • the accurate measurement of the neutrino interaction final states. Though most of the
528 muons will be reconstructed and identified in the MRDs, the hadronic particles will
529 predominantly stops in one WAGASCI module. One has therefore to rely exclusively

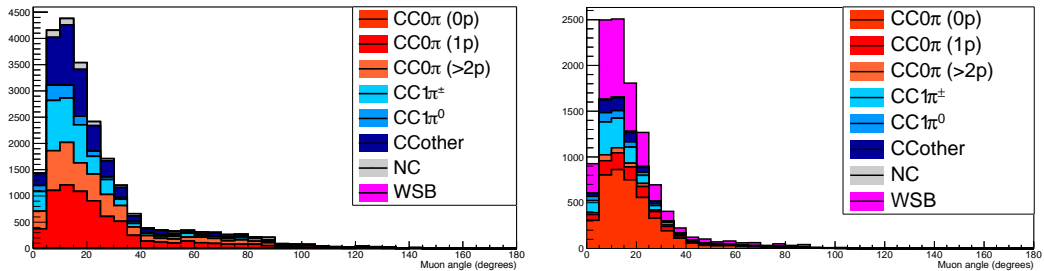


Figure 25: The reconstructed angles of the longest tracks in the selected events in the neutrino-mode (left) and the antineutrino-mode (right).

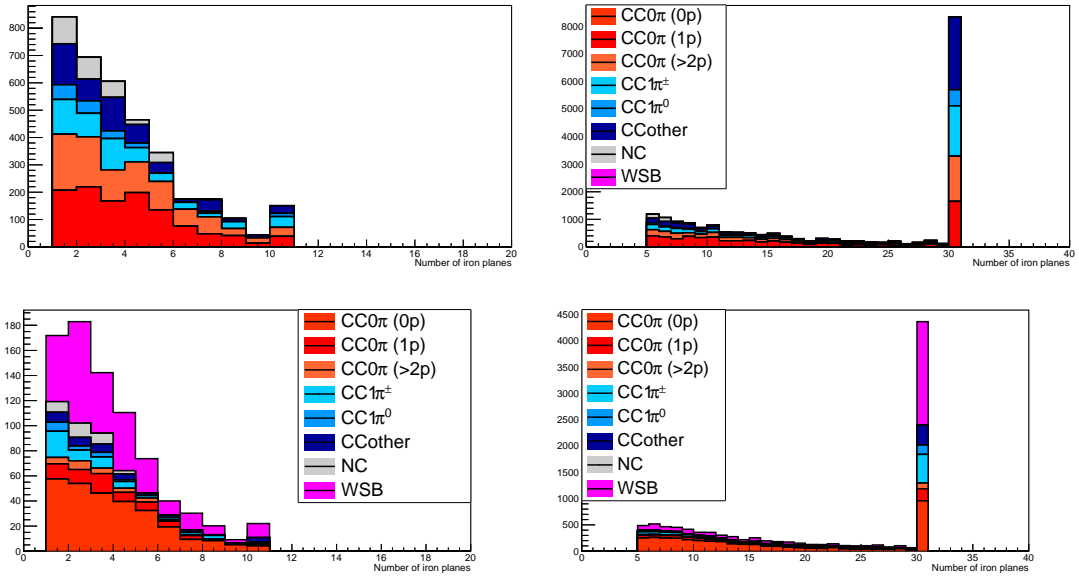


Figure 26: Iron plane numbers in Side-MRD (left) and Baby-MIND (right) corresponding to the end points of the longest tracks in the selected events in the neutrino-mode (top) and the antineutrino-mode (bottom).

530 on the WAGASCI module information alone to reconstruct, identify and measure the
 531 momentum of pions or protons.

- 532 • the coverage of the MRDs is not 4π . Using the WAGASCI module information can
 533 therefore help to constraint the particles that exits the WAGASCI module but do
 534 not geometrically enters any MRD.
- 535 • the particle identification of low momenta muons $p_\mu < 300 \text{ MeV}/c$ that will leave only
 536 few hits in the MRD. Using the WAGASCI module information will clearly enhance
 537 the particle identification.

538 This study is based on an original study done for the ND280 upgrade target, with some
 539 modifications. Though the cell size is similar to the WAGASCI configuration presented
 540 in Section 5, the external dimensions are different ($186.4 \times 60 \times 130 \text{ cm}^3$). Whenever the
 541 results are presented with this external size and this parameter is likely to impact the
 542 result, it will be mentioned.

543 Note that in this section, a simplified reconstruction algorithm presented in Section 6.1 is
 544 used. The fiducial volume is chosen accordingly as the inner cube of the module which
 545 surfaces are distant of $4 \times$ scintillator space = 10 cm from the module external surfaces.

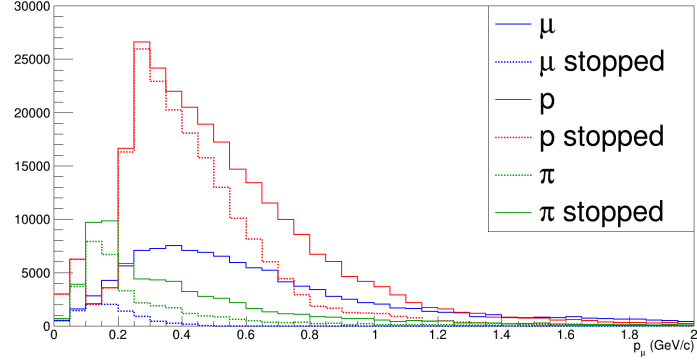


Figure 27: Momentum distribution of true particles in WAGASCI (plain) and corresponding distributions only for particles stopping into the WAGASCI module (dashed).

546 The neutrino interactions are simulated using NEUT v5.3.2. The NEUT input neutrino
 547 flux is estimated using JnuBeam v13a and assuming the detector to be located at 1.5°
 548 off-axis, as in Section 5. Note that the event reconstruction efficiency as a function of true
 549 neutrino energy might be changed at 1.5° , due for example to different Q^2 distributions. For
 550 this reason, one has to note that the reconstruction results might slightly be changed from
 551 2.5° and 1.5° . To avoid a similar change on the particle-only reconstruction efficiencies,
 552 they will be presented as a function of variables that completely characterize the particle
 553 kinematic state, *i.e.* its momentum and angle. Figure 28 shows the vertices distributions
 554 of the daughter particles of neutrinos interacting one standard WAGASCI water-module.
 555 In this section, we will show the detector reconstruction and particle identification in this
 556 phase space, both for leptonic and hadronic particles. We will finally show an empty
 557 WAGASCI module can highly enhance the ability to constrain the neutrino interaction
 558 final state which is critical to reduce the corresponding uncertainties.

559 6.1 Reconstruction algorithm

560 6.1.1 Description

561 For this section, an ideal ‘‘simulated’’ reconstruction is developed. A particle is recon-
 562 structed if:

- 563 1. The particle is charged.
- 564 2. Lets at least one hit (energy deposit > 2.5 photo-electron) in a scintillator.
- 565
- 566 3. The particle enters one TPC and let one hit in the tracker.

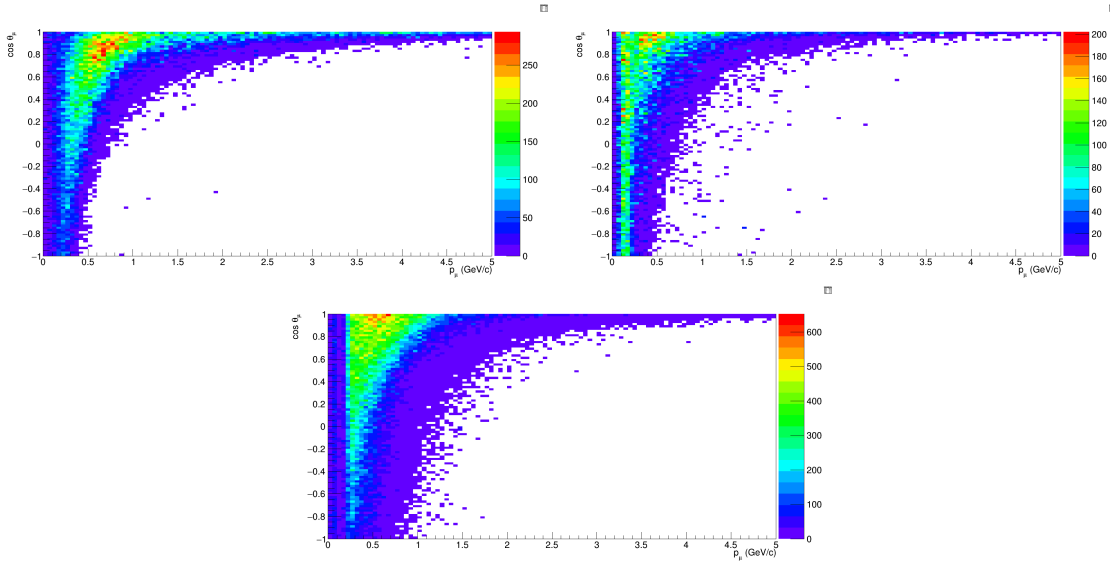


Figure 28: True number of muons (left), charged pions (right) and protons (bottom) in the two WAGASCI water-module as a function of the particles momenta and angles at 1.5° .

567 Or

568

569

- 570 • The particle should be long enough to be reconstructed by the detector in at least 2 out of 3 views (XZ, YZ, XY). The length criterion requires the particle to let at least 4 hits in the detector. In the “less favourable case” of pure longitudinal or transverse going tracks, it represents a the track length of $L_{track} \geq 4 \times$ scintillator space = 10.0 cm.
- 571
- 572
- 573
- 574 • In the views where particles pass the length criterion, the particle shall not be superimposed with longer tracks in at least two views. The superposition criterion is estimated with the distance inter-tracks (DIT) which corresponds to the orthogonal distance between two tracks at the ending point of the shortest one (see Figure 29). For a track 1, the superposition criterion is tested with every longer tracks that starts at the same vertex. Let \vec{p}_1 the vector of track 1, and p_1^a its projections in the XZ, YZ and XY planes respectively for $i=1,2,3$. Note that these are projections in a 2D planes and not on a direction vector. In this case, the relative angle between the track 1 and a longer track 2 (of vector \vec{p}_2) in a view a is given by:
- 575
- 576
- 577
- 578
- 579
- 580
- 581
- 582
- 583

$$\cos \theta = \frac{\vec{p}_1^a \cdot \vec{p}_2^a}{\|\vec{p}_1^a\| \|\vec{p}_2^a\|} \quad (1)$$

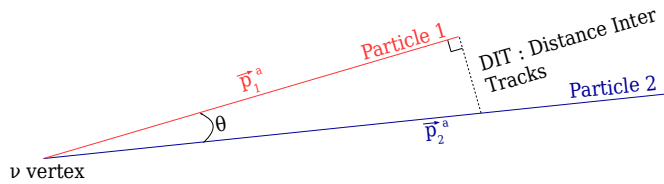


Figure 29: Definition of the distance inter tracks.

584 and the distance inter track is given by:

$$585 \quad DIT = ||\vec{p}_1^a|| \sin \theta \quad (2)$$

586 The DIT should be higher than $4 \times$ scintillator width for the track 1 to be not
 587 superimposed with the track 2 in the view a, which also corresponds to 10.0 cm
 in the nominal configuration.

588 **6.1.2 Performances**

589 The particle-only reconstruction efficiencies and the reconstruction threshold in momenta
 590 are shown in Table 4. This threshold is defined as the maximal momentum for which the
 591 reconstruction efficiency is smaller than 30%. The thresholds in muon and pion momenta
 592 are 150 MeV/c. Most of the muons are above this threshold (see Figure 28) which leads
 593 to a 79% reconstruction efficiency.

	μ	π	p
Reconstruction Efficiency	79%	52%	26%
Momentum threshold	150 MeV/c	150 MeV/c	550 MeV/c

Table 4: Reconstruction efficiency and momentum threshold for muons, pions and protons.
 The threshold is defined as the maximal momentum for which particles have a reconstruction efficiency smaller than 30%.

594 The lower pion and proton efficiencies (respectively 52% and 26%) are due to lower
 595 efficiencies for similar momenta than muons, coming from strong interactions as shown
 596 on Figures 30. Efficiencies of each particle type tend to decrease in the backward region
 597 due to particle lower momenta. However, for a fixed momentum value, the reconstruction
 598 efficiency is almost uniform which confirms the ability of the WAGASCI detector to
 599 reconstruct high angle tracks.

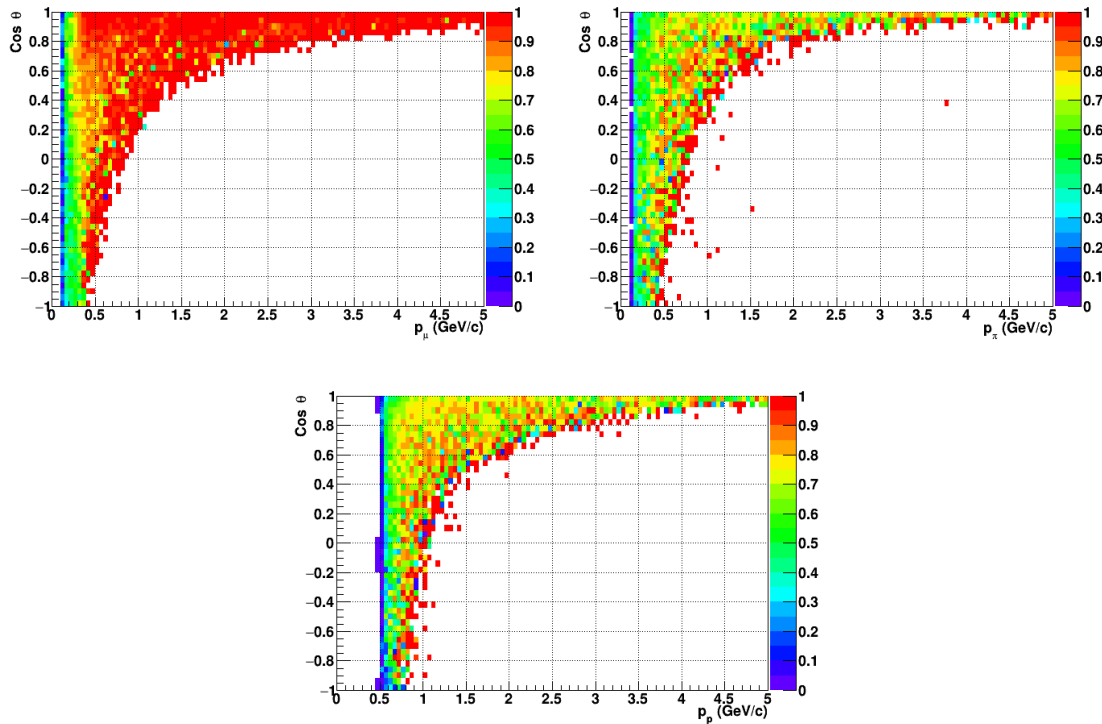


Figure 30: Reconstruction efficiency of muons (left), charged pions (right) and protons (bottom) in the WAGASCI water-module as a function of the particles momenta and angles.

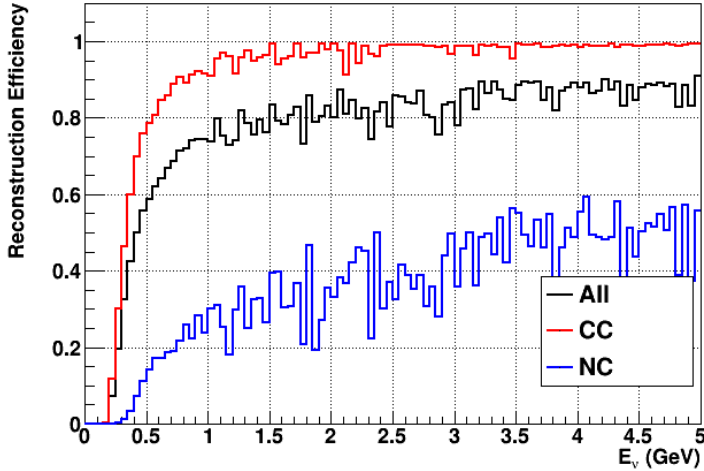


Figure 31: Reconstruction efficiency of all neutrino (black), CC (red) and NC (blue) interactions in the WAGASCI water-module as a function of the neutrino energy.

600 The reconstruction is thereafter tested on neutrino events. Table 5 summarizes the
 601 number of reconstructed events and efficiencies for each interaction type. As expected
 602 from the high muon reconstruction efficiency, the charged current interactions have recon-
 struction efficiencies $\geq 85\%$.

	CC0 π	CC1 π	CCOthers	NC	All
Reconstruction efficiency	85%	87%	91%	22%	68%

Table 5: Number of true interactions reconstructed. The purity and reconstruction effi-
 ciency of each true interaction is also shown.

603
 604 The reconstruction efficiencies as a function of the neutrino energy and muon kinematics
 605 are respectively shown on Figure 31 and 32.

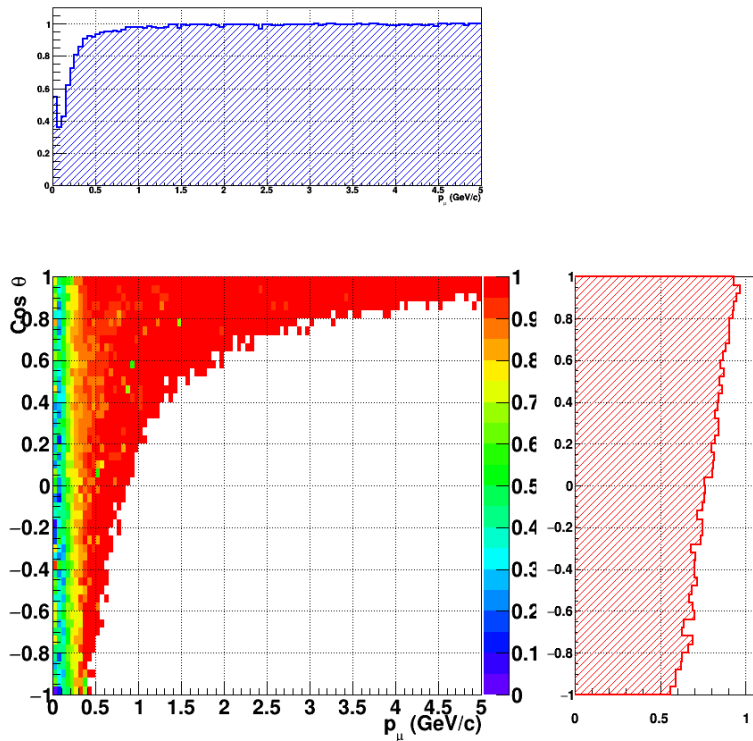


Figure 32: Reconstruction efficiency of CC interactions in the WAGASCI water-module as a function of the muon kinematic variables (momentum and angle).

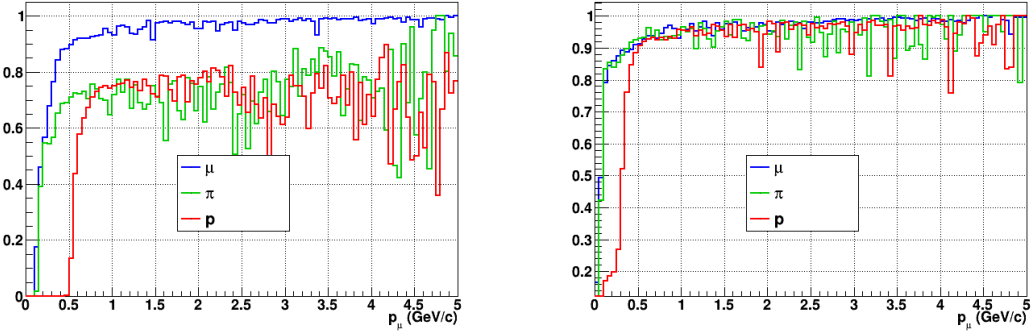


Figure 33: Reconstruction efficiency for muons, pions and protons in the water-in (left) and water-out (right) modules.

Note that a Particle Identification Algorithm has been also developed. It is based on the charge deposition of the particles in the scintillator, of the detection of a decay-electron. However, this information highly depends on the number of scintillator hit by a particle, which creates an important difference between a real WAGASCI module and the one used for the ND280-upgrade simulation. For this reason, the corresponding results will not be detailed here, but can be found in [?].

6.2 Background subtraction: the water-out module

In the nominal configuration, 20% of the neutrino interactions occurs on scintillators (C_8H_8). This background should be removed in order to measure the neutrino interaction on the same target as Super-K, which suppress the differences in cross-section models. For this purpose, we propose to use a water-out module, where the water is replaced by air. The detector is therefore fully active and has a 3 mm spatial resolution (scintillator thickness) which create an ideal detector to reconstruct and identify hadrons, and study np-nh interactions. The counter-part is the difference in particle energy deposition between the water and this water-out module that will need to be corrected for. In this section, we present the capabilities of such a module, and the impact it can have on cross-section measurements for the neutrino community in general and T2K in particular. The same reconstruction and selection as the water-in module is applied. Figure 33 shows the comparison between the water-in and the water-out reconstruction efficiencies for muon, pions and protons. 90% of the muons and 87% of the pions are reconstructed, while 70% of the protons are even reconstructed. It allows to lower down the proton threshold to 250 MeV/c (see Table 6).

As a consequence of tracking even low momenta particle, the reconstruction efficiency is uniform and almost maximal on the entire $\cos \theta_\mu$ phase space, as shown on Figure 34.

	μ	π	p
Reconstruction Efficiency Momentum threshold	90% 50 MeV/c	87% 50 MeV/c	70% 250 MeV/c

Table 6: Reconstruction efficiency, proportions of μ -like and non μ -like and momentum threshold for muons, pions and protons in the empty module. The threshold is defined as the maximal momentum for which particles have a reconstruction efficiency smaller than 20%.

630 Since the fiducial mass represents 0.25 tons, the total number of events is divided by a
 631 factor of 3 compared to the water-in module. The water-out module offers interesting
 632 possibilities to study np-nh interaction since 70% of the protons are reconstructed. In the
 633 future, a possible separation as a function of the number of proton track will be studied.
 634 Moreover, we are currently pursuing the use of single and double transverse variables (cite
 635 Xianguo) to open new possibilities for separating np-nh from Final State Interactions, or
 636 for isolating the interactions on hydrogen from interactions on carbon in this module.

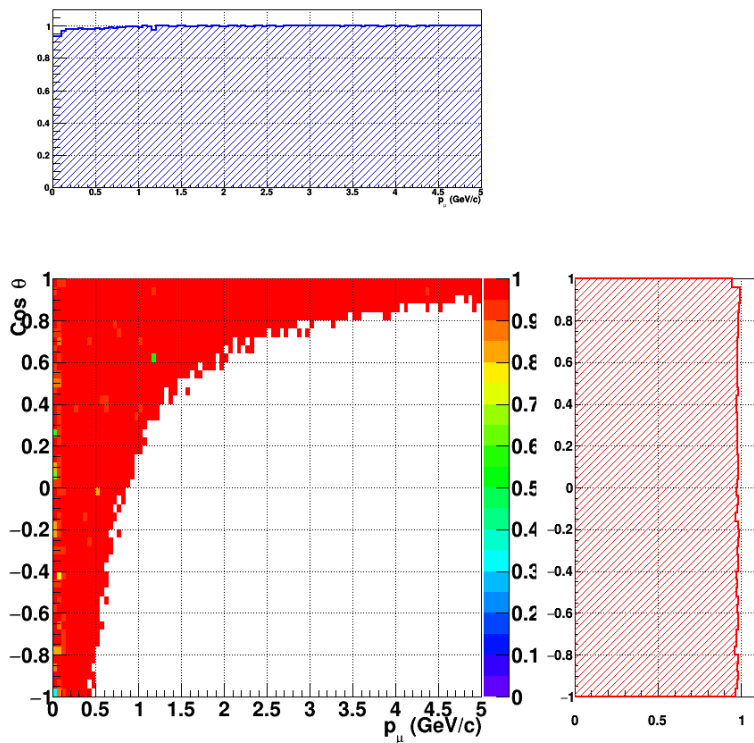


Figure 34: Reconstruction efficiency of CC interactions in the WAGASCI empty module as a function of the muon kinematic variables (momentum and angle).

637 **7 Schedule**

638 We would like to start a physics data taking from T2K beam time after the summer
639 shutdown in 2018. By then, commissioning and tests of the detectors will be completed
640 in J-PARC T59. The experiment can run parasitically with T2K, therefore we request no
641 dedicated beam time nor beam condition as discussed in the following section.

642 Once the approved POT is accumulated, the WAGASCI modules will be removed
643 from the experimental site, but we would like to keep the Baby-MIND and the Side-MRD
644 modules on the B2 floor of the NM pit as common platforms of future neutrino experiments
645 using the T2K neutrino beam.

646 **8 Requests**

647 **8.1 Neutrino beam**

648 The experiment can run parasitically with T2K, therefore we request no dedicated beam
649 time nor beam condition. As data taking periods, we request the ‘nominal’ T2K one-year
650 operation both for the neutrino beam and the antineutrino beam. The T2K has been
651 requesting 0.9×10^{21} POT/year and actually accumulating about 0.7×10^{21} POT/year in
652 recent years. For each year, starting from the Autumn, T2K is running predominantly in
653 the neutrino mode or in the antineutrino mode. Our request is to have one-year neutrino-
654 mode data and another one-year antineutrino mode data assuming that the POT for the
655 fast extraction in each year is more than 0.5×10^{21} POT.

656 **8.2 Equipment request including power line**

657 We request the followings in terms of equipment on the B2 floor:

- 658 • Site for the WAGASCI modules, Side-MRD modules and BabyMIND and their elec-
659 tronics system on the B2 floor of the near detector hall (Figure 2 and 3).
- 660 • Anchor points (holes) on the B2 floor to secure the WAGASCI modules, Side-MRD
661 module and Baby-MIND, detailed floor plans to be communicated in a separate
662 document.
- 663 • Power line for the magnets in Baby-MIND: 400 V tri-phase 48-to-62 Hz, capable of
664 delivering 12 kW. We have a wish for the magnet power line to be installed and
665 available to us by beginning of March 2018.
- 666 • Electricity for electronics and water circulation system, 3 kW, standard Japanese
667 electrical sockets.

- 668 1. Online PCs: 2.1 kW

669 2. Electronics: 0.7 kW

670 3. Water sensors: 1 kW

- 671 • Air conditioner for cooling heat generation at Baby-MIND magnets, online PCs and
672 electeronics
- 673 • Beam timing signal and spill information
- 674 • Network connection

675 The infrastructure for much of the above exists already. Exceptions are the power line
676 for the magnet and the electronics and holes in the B2 floor to anchor the detector support
677 structures.

678 References

- 679 [1] K. Abe et al. Measurement of the muon neutrino inclusive charged-current cross
680 section in the energy range of 13 GeV with the T2K INGRID detector. *Phys. Rev.*,
681 D93(7):072002, 2016.
- 682 [2] M. Antonova et al. Baby MIND Experiment Construction Status. In *Prospects in*
683 *Neutrino Physics (NuPhys2016) London, London, United Kingdom, December 12-14,*
684 2016, 2017.
- 685 [3] K. Nitta et al. The k2k scibar detector. *Nucl. Instrum. Meth. A*, 535:147, 2004.
- 686 [4] K. Abe et al. (T2K Collaboration). Measurement of the inclusive ν_μ charged current
687 cross section on iron and hydrocarbon in the t2k on-axis neutrino beam. *Phys. Rev.*
688 D, 90:052010, 2014.
- 689 [5] F. Magniette F. Gastaldi, R. Cornat and V. Boudry. A scalable gigabit data acquisition
690 system for calorimeters for linear collider. *proceedings of TIPP2014*, page PoS 193,
691 2014.
- 692 [6] J. Fleury, S. Callier, C. de La Taille, N. Seguin, D. Thienpont, F. Dulucq, S. Ahmad,
693 and G. Martin. Petiroc and Citiroc: front-end ASICs for SiPM read-out and ToF
694 applications. *JINST*, 9:C01049, 2014.
- 695 [7] M. B. Barbaro J. A. Caballero T. W. Donnelly G. D. Megias, J. E. Amaro. Inclusive
696 electron scattering within the susav2 meson-exchange current approach. *Phys. Rev.*
697 D, 94:013012, 2016.
- 698 [8] M. Valverde J. Nieves, J. E. Amaro. Inclusive quasi-elastic neutrino reactions. *Phys.*
699 *Rev. C*, 70:055503, 2004.

- 700 [9] Yu. G. Kudenko, L. S. Littenberg, V. A. Mayatsky, O. V. Mineev, and N. V. Ershov.
701 Extruded plastic counters with WLS fiber readout. *Nucl. Instrum. Meth.*, A469:340–
702 346, 2001.
- 703 [10] O. Mineev, Yu. Kudenko, Yu. Musienko, I. Polyansky, and N. Yershov. Scintillator
704 detectors with long WLS fibers and multi-pixel photodiodes. *JINST*, 6:P12004, 2011.
- 705 [11] Etam Noah et al. Readout scheme for the Baby-MIND detector. *PoS*, Photo-
706 toDet2015:031, 2016.
- 707 [12] Omega. Spiroc 2 user guide. 2009.